
Anatomy of Capability Emergence: Scale-Invariant Representation Collapse and Top-Down Reorganization in Neural Networks

Jayadev Billa[†]
 San Jose, CA, USA
 jbill2004@gmail.com

Abstract

Capability emergence during neural network training remains mechanistically opaque. We track five geometric measures across five model scales (405K–85M parameters), 120+ emergence events in eight algorithmic tasks, and three Pythia language models (160M–2.8B). We find: (1) training begins with a universal representation collapse to *task-specific floors* that are scale-invariant across a 210× parameter range (e.g., modular arithmetic collapses to $\text{RANKME} \approx 2.0$ regardless of model size); (2) collapse propagates *top-down* through layers (32/32 task×model consistency), contradicting bottom-up feature-building intuition; (3) a *geometric hierarchy* in which representation geometry leads emergence (75–100% precursor rate for hard tasks), while the local learning coefficient is synchronous (0/24 precursor) and Hessian measures lag. We also delineate prediction limits: geometric measures encode coarse task difficulty but not fine-grained timing (within-class concordance 27%; when task ordering reverses across scales, prediction fails at 26%). On Pythia, global geometric patterns replicate but per-task precursor signals do not—the precursor relationship requires task-training alignment that naturalistic pre-training does not provide. Our contribution is the geometric anatomy of emergence and its boundary conditions, not a prediction tool.

1 Introduction

Capability emergence, the sudden appearance of new abilities during neural network training, remains one of the least understood phenomena in deep learning [Wei et al., 2022]. Despite growing interest in predicting when models will acquire specific capabilities (for both scientific understanding and safety monitoring), progress has been hampered by a fundamental gap: we lack a systematic understanding of *how the internal geometry of neural networks changes as capabilities emerge*. Three relevant literatures have developed largely in isolation. Work on representation geometry has revealed developmental phases during training [Li et al., 2025, Belrose et al., 2024], loss landscape analysis has characterized curvature evolution [Ghorbani et al., 2019, Sagun et al., 2018], and singular learning theory has proposed the local learning coefficient as a training progress measure [Watanabe, 2009, Lau et al., 2025, Hoogland et al., 2024]. But no study has systematically compared these geometric perspectives for their temporal relationship with capability emergence, tested whether geometric measures can predict which capability will emerge when, or examined how these relationships scale.

We address this gap with the most comprehensive geometric analysis of capability emergence to date. We design a controlled algorithmic emergence platform: five model scales spanning a 210× parameter range (405K to 85M), 24 capabilities across eight tasks at three difficulty levels, and dense checkpointing (~ 206 checkpoints per model), yielding 120 emergence events with known timing. We track five geometric measures (representation effective rank, Fisher eigenspectrum, local

[†]Unaffiliated researcher - previously at ISI@USC, Yahoo, Nuance, BBN.

learning coefficient, Hessian eigenvalues, gradient covariance rank) across these checkpoints. While the 120 events share correlation structure (levels of the same task and adjacent model sizes are not independent), they provide a rich testbed far beyond prior work. We then test whether these findings transfer to three Pythia language models (160M, 410M, 2.8B) using task-specific diagnostic sets. Unlike Li et al., who characterize global representation geometry phases, we perform *task-conditioned* geometric analysis, compare five geometric frameworks head-to-head, and quantitatively test predictive power.

Our analysis reveals a coherent geometric anatomy of capability emergence in the controlled setting, along with clearly delineated limits of geometric prediction:

1. *A controlled emergence platform* (§3.1). Eight algorithmic tasks spanning a genuine complexity hierarchy (copy through multiplication) with three difficulty levels, trained on five model sizes. This yields 120 emergence events with known timing, providing the first large-scale testbed for geometric analysis of emergence.
2. *Task-specific collapse floors* (§4.2). Training begins with a universal representation collapse. The floor of this collapse is task-specific: modular arithmetic collapses to $\text{RANKME} \approx 2.0$ regardless of model size (coefficient of variation $\text{CV} = \text{std}/\text{mean} = 0.08$), while tasks with higher intrinsic dimensionality show capacity-dependent floors. We interpret this as a minimum representational complexity that interacts with model scale.
3. *Top-down layer propagation* (§4.3). The collapse propagates top-down: output-facing layers collapse most, early layers maintain diversity. This holds with 32/32 consistency across task \times model combinations, contradicting the bottom-up feature-building intuition.
4. *A geometric hierarchy* (§4.4). Representation geometry (RANKME) leads behavioral emergence (precursor rate 75–100% for hard tasks—those requiring $>1,000$ training steps—across model scales), the local learning coefficient is synchronous (0/24 precursor) in our multi-task setting, and global Hessian lags. The cheapest measure provides the best temporal signal.
5. *Clearly delineated prediction limits* (§4.5). Despite the temporal hierarchy, geometric measures do not achieve fine-grained prediction. The overall correlation between early RANKME and emergence ordering ($\rho = 0.57\text{--}0.90$) is driven by easy-versus-hard task separation that task definitions already provide. Within difficulty classes, concordance drops to 27% (easy) and 78% (hard), and the swap test fails at 26%.

On Pythia, the collapse pattern and cross-benchmark RANKME ordering replicate qualitatively, but task-specific precursor signals are inconsistent (§4.6). The precursor relationship requires clean task boundaries that naturalistic pre-training does not provide, an important boundary condition for any geometric monitoring approach.

Our contribution is the comprehensive geometric anatomy (collapse floors, top-down propagation, the temporal hierarchy, and the bifurcation between easy and hard emergence) together with honest reporting of where geometric prediction succeeds and where it fails. We provide the map, not the destination.

2 Related Work

Representation geometry during training. Li et al. [2025] track the eigenspectrum of hidden-state covariance matrices across Pythia training and identify three developmental phases: representational collapse, entropy-seeking expansion, and compression-seeking consolidation. Our work replicates their three-phase finding on Pythia and extends it in three directions: (1) we perform *task-conditioned* geometric analysis rather than global representation geometry, revealing task-specific collapse floors; (2) we compare representation geometry against four other geometric frameworks (Fisher, LLC, Hessian, gradient covariance) for temporal precedence, a head-to-head comparison absent from their study; and (3) we quantitatively test whether geometric measures can *predict* emergence timing, not just describe it. Belrose et al. [2024] demonstrate that language models learn statistics of increasing complexity during training, which aligns with our finding of progressive representation diversification post-collapse, though their focus is on probing complexity rather than geometric measures.

Loss landscape geometry. The Hessian eigenspectrum has been extensively studied as a characterization of the loss landscape [Ghorbani et al., 2019, Sagun et al., 2018, Popyan, 2018], revealing a bulk-plus-outlier structure that evolves during training. Loss barriers between adjacent checkpoints [Vlaar and Frankle, 2022] provide a complementary view of landscape connectivity. Our

Table 1: Algorithmic tasks and difficulty scaling. All tasks use the format `TASK input = output`. Difficulty increases with level via input length or numerical range.

Task	Description	L1	L2	L3
COPY	Copy tokens	3 tokens	5 tokens	8 tokens
REV	Reverse tokens	3 tokens	5 tokens	8 tokens
CMP	Compare two numbers	1 digit	2 digits	3 digits
PAR	Parity of bits	4 bits	6 bits	8 bits
ADD	Addition	1+1 digit	2+2 digits	3+3 digits
MOD	Modular arithmetic	$p \in \{2, 3, 5, 7\}$	$p \in \{7, 11, 13\}$	$p \in \{13, 17, 19, 23\}$
SORT	Sort numbers	3 numbers	5 numbers	8 numbers
MUL	Multiplication	1×1 digit	1×2 digits	2×2 digits

contribution is not new geometric measures but a systematic temporal comparison: when do these different geometric lenses respond relative to behavioral emergence?

Singular Learning Theory. Watanabe [2009] establishes that singular models (where the Fisher information matrix is degenerate) require a geometric characterization beyond the Hessian. The local learning coefficient λ generalizes the classical notion of model dimension to singular settings. Lau et al. [2025] develop practical estimators for λ via SGLD sampling and propose it as a progress measure for training. Hoogland et al. [2024] apply LLC to detect developmental stages in GPT-2 training, finding that LLC transitions precede behavioral changes. Our work provides a more systematic comparison in a different regime: across 24 multi-task emergence events, LLC is synchronous with behavior (0/24 precursor rate). This does not invalidate the findings of Hoogland et al. [2024] in single-task settings, but indicates that LLC’s temporal relationship with emergence is context-dependent, an important boundary condition for its use as a generic monitoring tool.

Capability emergence. Wei et al. [2022] identify emergent abilities, capabilities that appear suddenly with increasing model scale, as a key phenomenon of large language models. Schaeffer et al. [2023] argue that apparent emergence is partly an artifact of nonlinear evaluation metrics, motivating our use of continuous log-probability metrics alongside accuracy. Nanda et al. [2023] identify interpretable progress measures (Fourier components, weight norms) that track grokking in modular arithmetic, demonstrating that mechanistic progress is visible before generalization. Our work extends this insight to a broader set of tasks and measures, finding that while representation geometry tracks progress, it does not achieve the fine-grained prediction Nanda et al.’s mechanistic measures provide for single-task grokking.

Pythia and training checkpoints. Biderman et al. [2023] release Pythia, a suite of 16 language models with 154 training checkpoints each, specifically designed to study training dynamics. Our analysis of three Pythia models (160M, 410M, 2.8B) provides cross-scale validation but reveals that naturalistic pre-training blurs the task-specific geometric signals clearly visible in controlled settings, an important methodological finding for future work using checkpoint suites.

3 Methods

3.1 Algorithmic Emergence Platform

We design a controlled experimental platform that provides dozens of emergence events with known timing and tunable difficulty in a single model. Eight algorithmic tasks span a genuine complexity hierarchy from memorization to multi-step computation (Table 1). Each task has three difficulty levels that scale the input size or numerical range, yielding 24 task×level combinations.

Model architecture. We use GPT-2-style decoder-only transformers [Radford et al., 2019] with pre-norm (LayerNorm before attention and FFN), GELU activations, learned positional embeddings, tied input/output embeddings, and no dropout. Five model sizes span a $210 \times$ parameter range (Table 2).

Training. AdamW optimizer with cosine learning rate schedule (1K-step warmup, peak LR 3×10^{-4} for nano–small, 1×10^{-4} for medium–large), weight decay 0.1, gradient clipping at 1.0, batch size 64. Training data is generated on-the-fly: each batch samples uniformly across all 8 tasks and 3 levels.

Table 2: Model configurations. Parameter counts exclude tied output embedding weights.

Size	Layers	d_{model}	Heads	d_{ff}	Parameters
Nano	2	128	4	512	405K
Micro	4	192	6	768	1.8M
Small	6	320	8	1,280	7.4M
Medium	8	512	8	2,048	25.2M
Large	12	768	12	3,072	85M

Table 3: Geometric measures used in this study. Cost is wall-clock time per checkpoint on the nano model (405K parameters); costs scale roughly linearly with parameter count for Fisher and Hessian.

Measure	Captures	Formulation	Cost
RANKME	Repr. dimensionality	$\exp(H(\bar{\sigma}))$, $\bar{\sigma}_i = \sigma_i / \sum_j \sigma_j$	~1s
Fisher eff. rank	Gradient concentration	$\exp(H(\bar{\lambda}^F))$ of Fisher eigenvalues	~85s
LLC	Loss landscape complexity	SGLD loss elevation $\hat{\lambda}$	~11s
Hessian top- λ	Global curvature	Stochastic Lanczos, $k=20$	~30s
Grad. cov. rank	Gradient diversity	Effective rank of $\nabla L \nabla L^\top$	~15s

Loss is masked to answer tokens only (positions after the = delimiter). Training runs for 100K steps (nano–small) or 200K steps (medium–large). Character-level tokenization with vocabulary size 41.

Checkpointing. Dense-where-it-matters schedule: every 100 steps for the first 10K steps, every 500 steps from 10K–50K, and every 2,000 steps from 50K onward, yielding ~206 checkpoints per model for 100K-step runs.

Evaluation. At every checkpoint, we evaluate all 24 task×level combinations on a fixed test set of 1,000 examples each (24,000 total). We record per-task accuracy, mean log-probability over correct answers, and per-item correctness flags. Following Schaeffer et al. [2023], we use continuous log-probability metrics alongside accuracy to avoid the emergence mirage.

Emergence detection. For the algorithmic experiment, our primary definition of emergence is the first training step at which accuracy exceeds 0.1 for ≥ 5 consecutive checkpoints (sustained exceedance). We choose this low threshold to capture the *onset* of non-trivial performance: for all eight tasks, chance-level performance is effectively zero (the output vocabulary is large enough that random guessing yields <0.01 accuracy), so sustained 10% accuracy represents a genuine qualitative transition. The consecutive-checkpoint requirement filters transient fluctuations. All emergence tables and precursor statistics in the main text use this definition. We verify robustness: raising the threshold to 0.5 shifts emergence steps by <15% for hard tasks and does not change the qualitative findings (see Appendix B). For Pythia, where per-task accuracy is not directly available, we use log-probability improvement over chance with sustained exceedance, consistent with the continuous-metric approach advocated by Schaeffer et al. [2023].

3.2 Geometric Measures

We measure five complementary geometric properties at each checkpoint, spanning representation geometry, gradient geometry, and loss landscape geometry (Table 3).

Task-specific RANKME. For each task, we collect hidden-state activations from the final transformer layer on 200 diagnostic examples, compute the singular value decomposition, and apply the RANKME formula [Garrido et al., 2023]: $\text{RankMe}(H) = \exp(-\sum_i \bar{\sigma}_i \log \bar{\sigma}_i)$, where $\bar{\sigma}_i = \sigma_i / \sum_j \sigma_j$ are the normalized singular values. This measures the effective dimensionality of the representation space as seen by each task. We also compute RANKME per transformer layer to study propagation patterns.

Fisher eigenspectrum. We compute per-sample gradients on 200 task-specific examples, form the gradient matrix $G \in \mathbb{R}^{N \times P}$ (N samples, P parameters), and eigendecompose the Gram matrix $GG^\top \in \mathbb{R}^{N \times N}$ to obtain the top- N eigenvalues of the empirical Fisher information matrix [Kunstner et al., 2019]. The Fisher effective rank is then $\exp(H(\bar{\lambda}^F))$ where $\bar{\lambda}^F$ are the normalized Fisher eigenvalues.

Table 4: Pythia diagnostic sets. Each set targets a different capability via specialized prompts. Unlike the algorithmic experiment, these are external probes into a model trained on heterogeneous text, not inputs from the training distribution.

Benchmark	Capability	Prompt format (example)	N
Syntactic	Subject–verb agreement	“The keys to the cabinet <i>is/are</i> ” (logprob)	36
Semantic	Word analogies	“man : woman :: king : ____” (4-way choice)	30
Arithmetic	Few-shot addition/mult.	“3+7=10; 15+23=38; 42+8=?” (3-shot)	200
ICL	In-context learning	Novel label mappings (4-shot sent./categ.)	16
Factual	Factual recall	“The capital of France is ____” (next token)	51
Logical	Deductive reasoning	“All dogs are animals. Rex is a dog. ∴ ____”	26
Pile	General text modeling	Random Pile validation sequences (perplexity)	200

Local Learning Coefficient (LLC). Following Lau et al. [2025], we estimate the LLC at each checkpoint using SGLD sampling: we run 500 SGLD steps with learning rate 10^{-5} , inverse temperature $\beta = 1.0$, and localization strength $\gamma = 10,000$, burning in the first 100 steps and computing the mean loss elevation relative to the checkpoint loss. The LLC measures the effective complexity of the loss landscape near the current parameter configuration.

Global Hessian. We compute the top-20 eigenvalues of the full-model Hessian via stochastic Lanczos quadrature [Ghorbani et al., 2019] using random Pile validation data. This captures global curvature structure independent of task-specific structure.

Gradient covariance rank. The effective rank of the batch-level gradient covariance matrix, measuring the diversity of gradient directions across training examples. For computational tractability, we compute this on the first 50K parameters, which biases toward embedding weights and early layers (see Appendix L for details and discussion of this limitation).

3.3 Pythia Generalization Probe

To test whether findings from the controlled algorithmic setting transfer to naturalistic language model pre-training, we analyze three Pythia-deduped models [Biderman et al., 2023]: 160M (154 checkpoints), 410M (154 checkpoints), and 2.8B (17 targeted checkpoints at steps 50K–80K, deliberately chosen to span the window around the known arithmetic phase change at step ~ 65 K).

For each Pythia checkpoint, we compute task-specific RANKME on seven diagnostic sets spanning the standard NLP capability hierarchy from syntax to reasoning (Table 4). Each set uses prompts designed to elicit capability-specific representations, enabling per-task geometric measurement analogous to the algorithmic experiment.

A critical asymmetry distinguishes the two settings. In the algorithmic experiment, diagnostic inputs are drawn from the model’s own training distribution: an input like ADD 23 45 = is both a training example and a diagnostic probe, so the representation geometry we measure is directly shaped by the training objective. For Pythia, our diagnostic sets are *external probes*—prompts constructed to target specific human-defined capabilities, but not necessarily aligned with Pythia’s training distribution (The Pile, a heterogeneous text corpus). This asymmetry is central to interpreting the Pythia results (§4.6).

We additionally use the full suite of global geometric measures (Hessian eigenvalues, loss barriers, gradient covariance, parameter statistics) computed at all 154 checkpoints for the 160M and 410M models.

3.4 Analysis Methods

Temporal precedence. For each (geometric measure, behavioral metric) pair, we compute the cross-correlation function (CCF) on first-differenced time series and identify the lag at which correlation peaks. A geometric measure is classified as a *precursor* if it peaks at negative lag (geometric change precedes behavioral change) with $|r| > 0.3$ (a conventional moderate-effect threshold; sensitivity checks at 0.2 and 0.4 yield qualitatively identical results).

Table 5: Emergence steps (training step at which accuracy exceeds threshold for ≥ 5 consecutive checkpoints) for 8 tasks across 5 model sizes. Easy tasks (gray) emerge during initialization; hard tasks (white) emerge later and show model-size dependence. L2 difficulty shown; L1/L3 follow the same pattern.

Task	Nano (405K)	Micro (1.8M)	Small (7.4M)	Medium (25.2M)	Large (85M)
COPY	200	200	200	200	200
REV	400	300	300	200	200
CMP	400	300	200	200	200
PAR	600	400	300	300	200
ADD	6,000	8,500	7,000	6,000	5,500
MOD	16,000	12,000	8,800	5,300	4,500
SORT	9,000	7,500	6,500	5,000	4,000
MUL	44,500	56,000	47,500	44,500	40,000

Precursor rate. The fraction of task \times model combinations for which a geometric measure is classified as a precursor. We report this across all tasks and separately for easy versus hard tasks.

State-based prediction. We test whether the geometric state at a fixed early checkpoint (the collapse floor) predicts the ordering of emergence across tasks. We compute Spearman rank correlations and concordance rates, with within-class stress tests that separate the contribution of coarse difficulty classification from fine-grained ordering.

4 Results

4.1 The Algorithmic Emergence Landscape

All 24 task \times level combinations achieve sustained emergence (accuracy exceeding threshold for ≥ 5 consecutive checkpoints) across all five model sizes, yielding 120 emergence events with known timing. While we report all 120 events, the effective number of independent observations is closer to 40 (8 tasks \times 5 scales), since difficulty levels provide correlated within-task replicates and adjacent model sizes share training dynamics. Emergence steps span over two orders of magnitude, from step 200 (MOD_L1, nano) to step 56,000 (MUL_L3, micro), providing a rich testbed for geometric analysis.

Tasks fall into two distinct categories based on when emergence occurs relative to the initial training dynamics (Table 5). *Easy tasks* (COPY, REV, CMP, PAR) emerge within the first 1,000 steps, during the universal initialization phase, with emergence timing that is largely insensitive to model size.¹ *Hard tasks* (ADD, MOD, SORT, MUL) require thousands to tens of thousands of steps, with emergence timing that depends on both task difficulty and model capacity: larger models consistently emerge earlier on hard tasks (e.g., MOD: 16K/12K/8.8K/5.3K steps for nano/micro/small/medium). At L2 difficulty, easy tasks emerge below 600 steps while hard tasks require at least 2,500 steps, creating a clear separation visible in Figure 1.

4.2 Universal Collapse to Scale-Invariant Floors

During the first 200 training steps, task-specific RANKME (effective dimensionality of hidden representations evaluated on each task’s diagnostic set; see §3.2) undergoes a sharp collapse across all tasks, all model sizes, and all layers. This collapse is not task-specific; it reflects a universal reorganization of initially random representations as training begins. The critical finding is that the *floor* of this collapse is task-specific (Figure 2), and for tasks with low intrinsic dimensionality, also scale-invariant.

¹One exception: PAR_L3 at the nano scale emerges at step 19,000, behaving like a hard task. At all larger model sizes PAR_L3 emerges below step 800. This outlier likely reflects the nano model’s limited capacity (2 layers, 405K parameters) for 8-bit parity, which requires tracking a global property across a relatively long input. We classify PAR as easy based on the dominant pattern across scales.

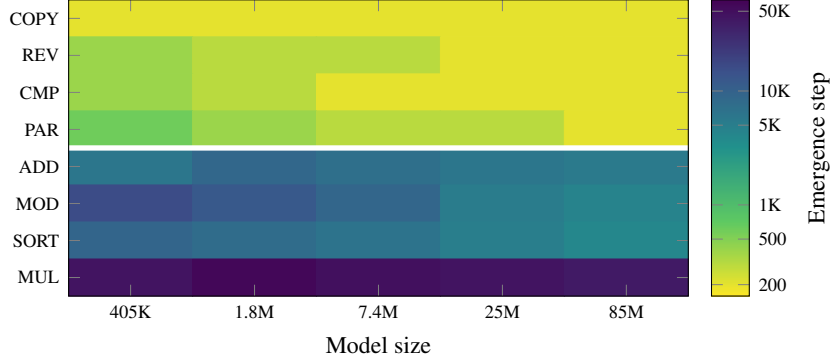


Figure 1: Emergence map. Log-scaled emergence step for 8 tasks across 5 model sizes. Easy tasks (above white line) emerge uniformly early regardless of scale; hard tasks (below) show scale-dependent acceleration. Color encodes $\log_{10}(\text{emergence step})$ using a sequential colormap.

Quantitatively, the collapse floor (minimum RANKME across early training) for each task, reported as mean \pm std across five model sizes:

- MOD: 2.12 ± 0.17 (CV = 0.08), robustly scale-invariant
- ADD: 3.93 ± 0.70 (CV = 0.18), approximately scale-invariant
- SORT: 6.16 ± 3.01 (CV = 0.49), floor increases with model capacity
- MUL: 5.25 ± 2.18 (CV = 0.42), floor increases with model capacity

Scale invariance is strongest for MOD, whose two-dimensional Fourier structure [Nanda et al., 2023] sets a hard floor of ~ 2 effective dimensions regardless of model size. For tasks with higher intrinsic dimensionality (SORT, MUL), larger models maintain higher minimum RANKME, suggesting they preserve more representational structure even at maximum compression. The collapse floor thus reflects an interaction between task complexity and model capacity, with tasks that have compact solutions showing true scale invariance.

Easy tasks emerge *during* this universal collapse window. Their emergence is essentially contemporaneous with the initial representation reorganization, which is why geometric precursors for easy tasks become indistinguishable from the universal initialization dynamics at larger model sizes (see §4.5).

Hard tasks emerge well after the collapse, during the subsequent recovery phase. The recovery trajectory following collapse is task-specific: ADD recovers to $\text{RANKME} \approx 8\text{--}12$ before emergence, while MUL continues growing to $\text{RANKME} > 15$ before achieving sustained accuracy. However, recovery magnitude is confounded with emergence timing ($\rho = 0.74$): harder tasks mechanically require both more recovery and more training steps, so the correlation reflects shared dependence on task difficulty rather than a causal relationship. Recovery *slope* does not predict within-model task ordering.

4.3 Top-Down Layer Propagation

Per-layer RANKME analysis reveals that the universal collapse propagates *top-down* through the network: the deepest (output-facing) layers collapse most, while early layers maintain greater representational diversity. This pattern holds with perfect consistency across all 32 task \times model combinations tested (8 tasks \times 4 model sizes with ≥ 4 layers), contradicting the intuition that learned features build bottom-up from simple to complex.

At the collapse minimum, the final transformer layer shows substantially lower RANKME than the first layer. For MOD: micro layer 0 = 8.2 vs. layer 3 = 1.7 (80% reduction), small layer 0 = 10.4 vs. layer 5 = 2.2 (78%), medium layer 0 = 14.8 vs. layer 7 = 2.3 (84%). The gradient is monotonic through layers: layer L collapses more than layer $L - 1$ for all L . Across all tasks and model sizes, the first-to-last-layer reduction ranges from 30% (easy tasks on small models, where overall collapse is mild) to 84% (hard tasks on larger models).

Post-emergence, the layer structure evolves: the final layer remains compressed (low RANKME) while middle layers recover and diversify. This creates a specialization-versus-diversity gradient,

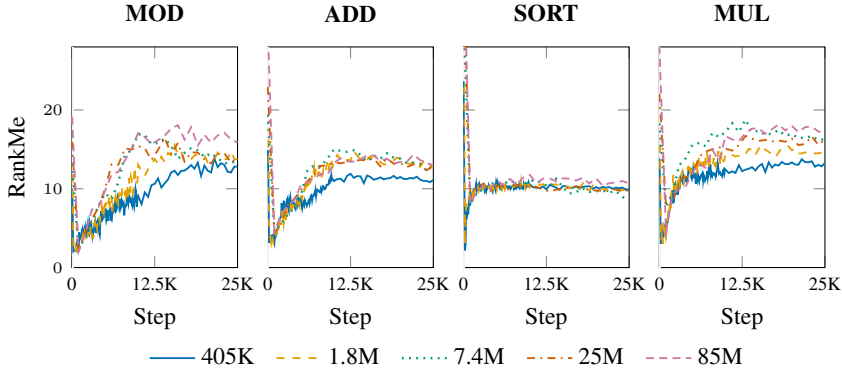


Figure 2: Task-specific collapse floors. RANKME trajectories for four hard tasks across five model sizes (405K–85M parameters). All models collapse to task-specific minima during initialization (steps 0–200, shaded), then recover at different rates. MOD shows robust scale invariance (floor ≈ 2.0 , CV = 0.08), while SORT and MUL floors increase with model capacity.

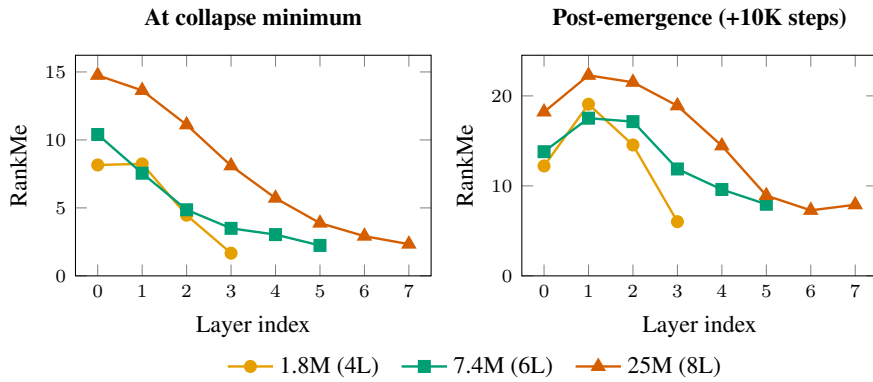


Figure 3: Top-down layer propagation. Per-layer RANKME at the collapse minimum (left) and post-emergence (right) for three model sizes on MOD. At collapse, deeper layers show lower RANKME (top-down gradient). Post-emergence, the final layer stays compressed while middle layers recover, creating a specialization-diversity gradient.

where output representations commit to task-relevant structure while intermediate representations maintain flexibility. The pattern suggests that the model commits output representations first, then adjusts intermediate features to support the committed output structure (Figure 3).

4.4 The Geometric Hierarchy

We compare five geometric measures for their temporal relationship with capability emergence. The measures span three levels of geometric abstraction: representation geometry (RANKME), gradient geometry (Fisher eigenspectrum), and loss landscape geometry (LLC, Hessian eigenvalues, gradient covariance rank). Table 6 and Figure 4 summarize the hierarchy.

RankMe leads. Task-specific RANKME detects geometric transitions before behavioral emergence in 86% of cases at the nano scale, with a median lead of ~ 700 training steps. The overall precursor rate degrades with model size (nano 86% \rightarrow micro 87.5% \rightarrow small 37.5% \rightarrow medium 25%), but this is driven entirely by easy tasks: they emerge during the universal collapse window at larger scales, where geometric and behavioral transitions become simultaneous. For hard tasks only, the precursor rate remains high across scales (nano 100%, micro 100%, small 75%, medium 75%). Easy tasks that “start emerged” at larger scales arguably should not be counted in the denominator; the hard-task rates better reflect RANKME’s genuine precursor power.

Table 6: Geometric hierarchy. Precursor rate = fraction of task \times model cases where the geometric transition precedes behavioral emergence. Rates are computed per task \times model pair; the effective number of independent tests is lower than the nominal count due to shared task structure across difficulty levels and adjacent model sizes. Cost measured on the nano model (405K parameters).

Measure	Level	Precursor Rate	Cost/ckpt	Temporal Relation
RANKME	Representation	86% (nano)	$\sim 1s$	Leads behavior
Fisher eff. rank	Gradient	$\sim 62\%$ (nano)	$\sim 85s$	Noisy, weak lead
LLC	Loss landscape	0% (0/24)	$\sim 11s$	Synchronous
Hessian top- λ	Global landscape	17%	$\sim 30s$	Noisy, lagging
Grad. cov. rank	Gradient	$\sim 50\%$	$\sim 15s$	Inconsistent

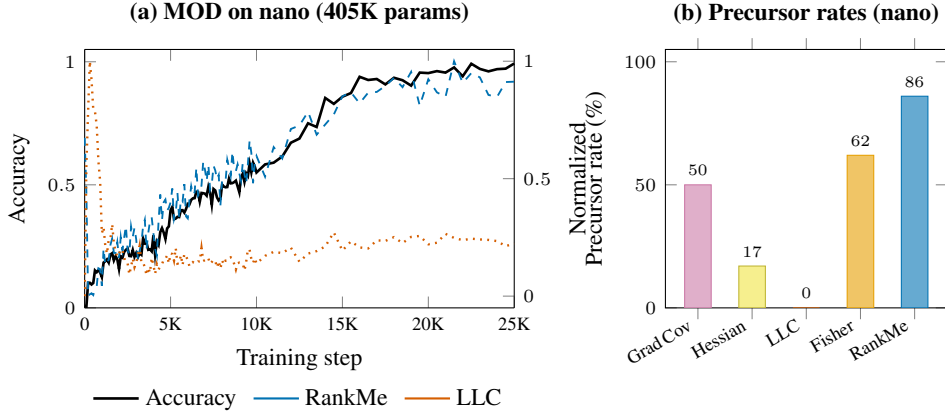


Figure 4: Geometric hierarchy. (a) Accuracy (left axis, black), RANKME (right axis, blue), and LLC (right axis, red) for MOD on nano (405K params). Both geometric measures are min-max normalized to [0,1] for visual comparison. RANKME collapses before emergence while LLC rises synchronously with accuracy. (b) Precursor rates across five geometric measures: RANKME leads in 86% of cases; LLC shows 0% precursor signal.

LLC is synchronous in this setting. The local learning coefficient [Lau et al., 2025], computed via SGLD sampling around each checkpoint, tracks task difficulty well (harder tasks have higher LLC) but shows *zero* precursor signal in our multi-task setting: 23/24 task-level combinations are synchronous with behavior (lag = 0), and 1/24 shows behavior leading LLC. This contrasts with prior single-task results [Hoogland et al., 2024] and suggests that LLC’s temporal relationship with emergence is context-dependent (see §5).

Fisher-LLC proxy fails. Singular learning theory predicts that the local learning coefficient equals half the Fisher effective rank at critical points [Watanabe, 2009]. This relationship holds approximately at convergence (step 50K+, ratio ≈ 1.0 for 3/4 tasks), but breaks down across the training trajectory ($\rho = 0.32$; per-task range $+0.04$ to $+0.46$). Nine denoising strategies (Appendix D) all yield $\rho \approx 0.28\text{--}0.35$, confirming this is not a noise artifact but a fundamental breakdown: Fisher captures local quadratic curvature while LLC captures the full singular geometry that dominates during learning (see Appendix K for the full convergence analysis).

Hessian is noisy. Global Hessian eigenvalues (stochastic Lanczos, $k = 20$) show only 17% precursor rate. The global measure averages over task-specific structure, diluting per-task signals.

The hierarchy reveals that the cheapest measure (RANKME, $\sim 1s$ /checkpoint) provides the strongest temporal signal, while more expensive loss landscape measures (LLC, Hessian) are concurrent or lagging. Representation geometry reorganizes *before* the loss landscape responds.

4.5 Prediction Limits

We test whether geometric measures can predict emergence *quantitatively*: not just that something will change, but *which* task will emerge *when*. We evaluate two prediction paradigms: event-based

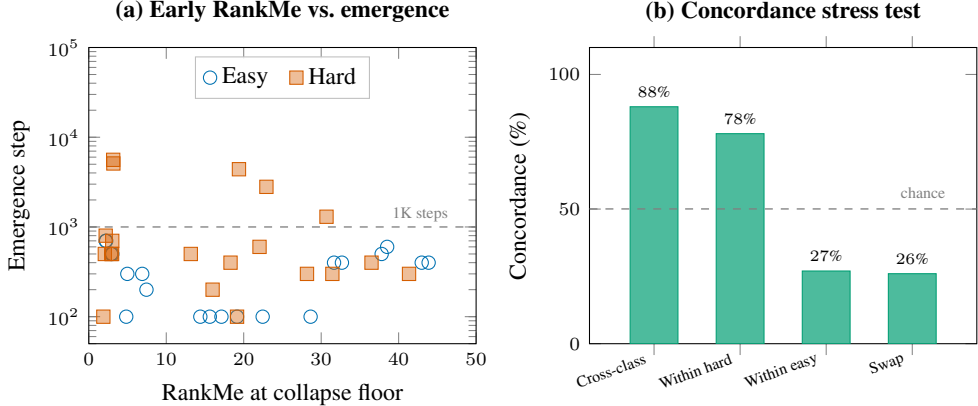


Figure 5: Limits of geometric prediction. (a) Early RANKME (at collapse floor) versus emergence step, colored by difficulty class. Within each class (easy = circles, hard = squares), RANKME does not reliably separate tasks. (b) Within-class concordance rates. Cross-class separation is strong (88%), but within-class prediction is weak: easy tasks score 27% (below the 50% chance line), and the swap test (predicting ordering changes across scales) fails at 26%.

detection (does a geometric transition precede emergence?) and state-based prediction (does early geometric state predict emergence ordering?).

Event-based detection. We test 13 geometric metrics (including RANKME transition timing, cross-task divergence, gradient alignment, eigenvalue concentration, and recovery statistics) as event-based precursors. No metric exceeds 69% precursor rate across all model sizes. The structural issue is that easy tasks emerge during the universal collapse window, making any initialization-phase geometric event appear simultaneous with emergence at larger scales. Event detection works well for hard tasks in small models but does not generalize.

State-based prediction. Early RANKME values (at the collapse floor) correlate with emergence ordering ($\rho = 0.57\text{--}0.90$ across model sizes). However, a within-class stress test reveals this correlation is driven primarily by the easy-versus-hard separation:

- *Cross-class concordance:* 88%. RANKME correctly separates difficulty classes, but so does the task definition itself.
- *Within hard tasks:* 78% concordance, largely driven by SORT being obviously easiest and MUL obviously hardest within the class.
- *Within easy tasks:* 27% concordance, *below chance*.
- *Swap test:* 26%. For task pairs whose emergence ordering reverses between model sizes (e.g., ADD emerges before MOD at one scale but after at another), early RANKME predicts the direction of the swap only 26% of the time.

Geometric measures encode a coarse difficulty ranking consistent with emergence ordering, but this ranking is largely redundant with what task definitions already reveal. The fine-grained prediction that would be practically useful (predicting *which specific capability* will emerge next in a model of a given size) is not achieved by any geometric measure we tested (Figure 5).

4.6 Do Structural Patterns Transfer to Naturalistic Pre-Training?

We test whether the algorithmic experiment’s findings transfer to naturalistic pre-training, using Pythia-160M and Pythia-410M (154 checkpoints each, 0–143K training steps) and Pythia-2.8B (17 targeted checkpoints, steps 50K–80K), with seven task-specific diagnostic sets (Table 4).

Collapse replicates. Task-specific RANKME drops 50–75% from step 0 to steps 64–128, then partially recovers, mirroring the algorithmic experiment’s universal initialization collapse. All seven benchmarks reach their RANKME minimum around steps 32–256 in both 160M and 410M.

RankMe ordering preserved. The RANKME ordering across benchmarks is perfectly consistent between model sizes: pile > logical > semantic > factual > syntactic > ICL > arithmetic (Spearman

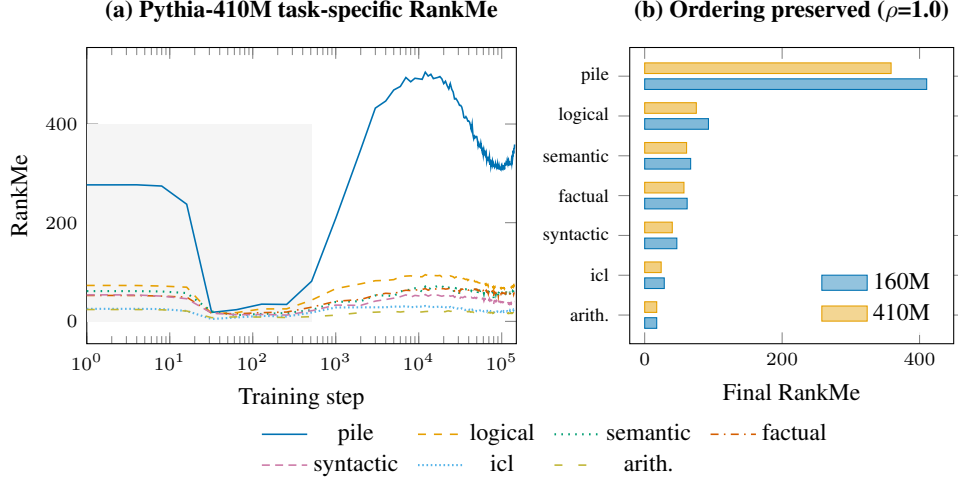


Figure 6: Pythia generalization probe. (a) RANKME collapse and recovery in Pythia-410M across seven benchmarks, replicating the algorithmic experiment’s universal collapse (shaded, steps 0–512). (b) Cross-model RANKME ordering is perfectly preserved ($\rho = 1.0$), but task-specific temporal precedence does not transfer.

$\rho = 1.0$ between 160M and 410M final-checkpoint values). The ordering reflects representation complexity: general text requires more effective dimensions than abstract reasoning, which requires more than specific pattern matching.

Late-training compression confirmed at 2.8B. All seven benchmarks show monotonic RANKME decline across steps 50K–80K at the 2.8B scale, confirming the third phase (collapse \rightarrow expansion \rightarrow compression) of the representation dynamics identified by Li et al. [2025]. No differential signal appears around the known arithmetic phase change at step \sim 65K.

Task-specific precursor: negative. Unlike the algorithmic experiment, task-specific RANKME does *not* consistently precede behavioral emergence on Pythia. In 160M, RANKME lags behavior; in 410M, results are mixed with sign inconsistencies across benchmarks. The critical difference is *task-training alignment*: in the algorithmic experiment, diagnostic inputs are drawn from the training distribution, so representation geometry is directly shaped by the training objective for each task. Our Pythia diagnostic sets are external probes (16–200 examples; Table 4) that target human-defined capabilities, but Pythia was trained on heterogeneous text without explicit task boundaries. Additionally, these sets are substantially smaller than the algorithmic experiment’s 1,000-example evaluations, yielding noisier RANKME estimates. The per-task precursor relationship thus requires task-training alignment that naturalistic pre-training does not provide—an important boundary condition, not a failure of geometric monitoring per se.

5 Discussion

Collapse floors as task complexity signatures. The task-specificity of collapse floors, and the strong scale invariance of the MOD floor ($CV = 0.08$ across a $210 \times$ parameter range), suggests these minima reflect a fundamental property of the task. We conjecture that the collapse floor corresponds to the minimum representational dimensionality required to distinguish task-relevant input classes. For modular arithmetic, two dimensions suffice because the task structure can be embedded in a circle (the Fourier basis for $\mathbb{Z}/p\mathbb{Z}$, as identified by Nanda et al. [2023] in the grokking context). For tasks with higher intrinsic dimensionality (SORT, MUL), the floor increases with model capacity ($CV \approx 0.4\text{--}0.5$), suggesting that larger models preserve more representational structure even at maximum compression. The interaction between task complexity and model capacity at the collapse floor is an important direction for future theoretical work: formalizing when floors are scale-invariant versus capacity-dependent could yield insight into task information content.

Why top-down, not bottom-up? The consistent top-down layer propagation (32/32 cases) contradicts the common intuition that neural networks learn simple features in early layers and compose them in later layers. Our finding suggests an alternative developmental sequence: the model first commits its output representations to be task-relevant (collapsing the output space to the task’s effective dimensionality), then adjusts intermediate features to support the committed output structure. This is consistent with the observation that post-emergence, the final layer remains compressed while middle layers recover; the output commitment is maintained while the supporting representations diversify.

LLC: context-dependent, not wrong. The local learning coefficient’s synchrony with behavioral emergence (0/24 precursor rate) in our multi-task setting contrasts with prior single-task results [Hoogland et al., 2024] where LLC tracked developmental stages. A natural interpretation: in our setting, LLC measures the complexity of the loss landscape that the model is *currently* navigating, which changes *because* the model is learning across many tasks simultaneously. Representation reorganization (RANKME collapse/recovery) is a prerequisite: the model must first rearrange its representations before the loss landscape reflects the new structure. This suggests strong context-dependence in LLC’s temporal relationship with behavior, and limits to using LLC as a generic early-warning signal without understanding the training regime.

Why global measures fail. Global Hessian eigenvalues (17% precursor rate) wash out task-specific signals because they aggregate across tasks with different loss scales and developmental phases. For a multi-task loss $L = \sum_i L_i$, the Hessian $H = \sum_i H_i$ is dominated by whichever task currently contributes most to curvature, obscuring early geometric transitions in individual tasks. This explains why task-specific representation geometry (RANKME) outperforms all global measures: it isolates per-task developmental dynamics that global quantities average away. The lesson for geometric monitoring is that the *granularity* of the measure must match the granularity of the capability of interest.

Why prediction is hard. The easy/hard bifurcation creates a structural obstacle: easy tasks emerge during the universal collapse, making their timing a property of initialization dynamics rather than task geometry, while hard tasks’ within-class ordering varies across model sizes (swap test: 26%). Geometric measures thus encode coarse difficulty, information that task definitions already provide, but not the fine-grained timing that would be practically useful. Overcoming this may require task-specific mechanistic measures [Nanda et al., 2023] rather than generic geometric ones.

The Pythia gap. The negative task-specific precursor result on Pythia is an important boundary condition. Naturalistic pre-training co-develops many capabilities simultaneously from overlapping training distributions, preventing the clean task-specific geometric signals that emerge in controlled settings. Our diagnostic sets (16–200 examples per benchmark; Table 4) may also underestimate Pythia’s internal task complexity. The positive results (collapse replication, preserved RANKME ordering, Phase 3 compression confirmation) demonstrate that the geometric *phenomena* are real across settings, even if the task-specific *precursor* relationship requires well-separated task boundaries.

Limitations. (1) *Task scope:* 8 algorithmic tasks, while spanning a genuine complexity hierarchy, are simpler than natural language tasks. The scale-invariant collapse floors may not hold for tasks with richer compositional structure. (2) *Model scale:* Our largest model (85M parameters) is small by current standards. Whether the geometric anatomy persists at frontier scale (>7B) remains open. (3) *Correlational evidence:* We establish temporal precedence but not causation. Intervening on representations (e.g. freezing specific layers during the collapse phase) would provide stronger evidence but is beyond the scope of this study. (4) *Task count:* The effective number of independent observations is ~ 40 (8 tasks \times 5 scales), with difficulty levels providing correlated replicates; fine-grained analyses (within-class concordance) are based on smaller subsets still. (5) *Gradient covariance:* We compute gradient covariance on a prefix of the first 50K parameters, biasing toward embedding weights and early layers (Appendix L). This may partly explain gradient covariance’s inconsistent precursor performance. (6) *Pythia diagnostics:* Our diagnostic sets (16–200 examples; Table 4) are small relative to the algorithmic experiment’s 1,000-example evaluations, and task-specific results may improve with larger, more carefully curated sets.

Future directions. Three questions emerge naturally: (1) Do scale-invariant collapse floors persist at frontier scale? If MOD \rightarrow 2.0 holds for models with billions of parameters, this would have practical implications for capacity planning. (2) Can causal interventions confirm the top-down developmental sequence? Freezing output layers during collapse and measuring the effect on emergence timing would directly test the output-commitment-first hypothesis. (3) What happens in instruction-tuned

models, where task boundaries are explicitly defined? The Pythia negative result may be reversed with clean task supervision.

6 Conclusion

We have presented the most systematic comparison of geometric measures during capability emergence to date, analyzing five geometric lenses across five model scales, 24 capabilities, and over 200 checkpoints per model. The data reveals three novel structural findings in the controlled setting: (1) universal representation collapse to task-specific floors, robustly scale-invariant for low-dimensionality tasks (MOD: CV = 0.08) and capacity-dependent for complex tasks; (2) top-down layer propagation with 32/32 consistency, where output layers commit before intermediate layers diversify; and (3) a temporal hierarchy in which representation geometry leads, loss landscape geometry (LLC) is concurrent in this multi-task setting, and global Hessian measures lag. The collapse pattern and cross-benchmark ordering replicate on Pythia language models at the phenomenological level.

We also clearly delineate where geometric monitoring fails. Geometry is necessary but not sufficient for fine-grained prediction: the predictive power of early RANKME values ($\rho = 0.57\text{--}0.90$ with emergence ordering) is largely contained in the coarse easy-versus-hard separation that task definitions alone already provide (cross-class concordance 88%, but within-easy 27%, swap test 26%). Event-based precursor detection does not scale beyond small models for easy tasks. Task-specific signals require clean task boundaries absent in naturalistic pre-training. These boundary conditions are as important as the positive findings: they define the scope within which geometric monitoring is informative and prevent premature claims about predictive capability.

The geometric anatomy of emergence (how representation collapse, layer propagation, and geometric hierarchies interact during learning) provides a structural foundation for future work on prediction, intervention, and mechanistic understanding of capability emergence.

References

- Nora Belrose, Quintin Pope, Lucia Quirke, Alex Mallen, and Xiaoli Z. Fern. Neural networks learn statistics of increasing complexity. In Ruslan Salakhutdinov, Zico Kolter, Katherine A. Heller, Adrian Weller, Nuria Oliver, Jonathan Scarlett, and Felix Berkenkamp, editors, *Forty-first International Conference on Machine Learning, ICML 2024, Vienna, Austria, July 21-27, 2024*, volume 235 of *Proceedings of Machine Learning Research*, pages 3382–3409. PMLR / OpenReview.net, 2024. URL <https://proceedings.mlr.press/v235/belrose24a.html>.
- Stella Biderman, Hailey Schoelkopf, Quentin Gregory Anthony, Herbie Bradley, Kyle O’Brien, Eric Hallahan, Mohammad Aflah Khan, Shivanshu Purohit, USVSN Sai Prashanth, Edward Raff, Aviya Skowron, Lintang Sutawika, and Oskar van der Wal. Pythia: A suite for analyzing large language models across training and scaling. In Andreas Krause, Emma Brunskill, Kyunghyun Cho, Barbara Engelhardt, Sivan Sabato, and Jonathan Scarlett, editors, *International Conference on Machine Learning, ICML 2023, 23-29 July 2023, Honolulu, Hawaii, USA*, volume 202 of *Proceedings of Machine Learning Research*, pages 2397–2430. PMLR, 2023. URL <https://proceedings.mlr.press/v202/biderman23a.html>.
- Quentin Garrido, Randall Balestrieri, Laurent Najman, and Yann LeCun. Rankme: Assessing the downstream performance of pretrained self-supervised representations by their rank. In Andreas Krause, Emma Brunskill, Kyunghyun Cho, Barbara Engelhardt, Sivan Sabato, and Jonathan Scarlett, editors, *International Conference on Machine Learning, ICML 2023, 23-29 July 2023, Honolulu, Hawaii, USA*, volume 202 of *Proceedings of Machine Learning Research*, pages 10929–10974. PMLR, 2023. URL <https://proceedings.mlr.press/v202/garrido23a.html>.
- Behrooz Ghorbani, Shankar Krishnan, and Ying Xiao. An investigation into neural net optimization via hessian eigenvalue density. In Kamalika Chaudhuri and Ruslan Salakhutdinov, editors, *Proceedings of the 36th International Conference on Machine Learning, ICML 2019, 9-15 June 2019, Long Beach, California, USA*, volume 97 of *Proceedings of Machine Learning Research*, pages 2232–2241. PMLR, 2019. URL <http://proceedings.mlr.press/v97/ghorbani19b.html>.

Jesse Hoogland, George Wang, Matthew Farrugia-Roberts, Liam Carroll, Susan Wei, and Daniel Murfet. The developmental landscape of in-context learning. *CoRR*, abs/2402.02364, 2024. doi: 10.48550/ARXIV.2402.02364. URL <https://doi.org/10.48550/arXiv.2402.02364>.

Frederik Kunstner, Philipp Hennig, and Lukas Balles. Limitations of the empirical fisher approximation for natural gradient descent. In Hanna M. Wallach, Hugo Larochelle, Alina Beygelzimer, Florence d’Alché-Buc, Emily B. Fox, and Roman Garnett, editors, *Advances in Neural Information Processing Systems 32: Annual Conference on Neural Information Processing Systems 2019, NeurIPS 2019, December 8-14, 2019, Vancouver, BC, Canada*, pages 4158–4169, 2019. URL <https://proceedings.neurips.cc/paper/2019/hash/46a558d97954d0692411c861cf78ef79-Abstract.html>.

Edmund Lau, Zach Furman, George Wang, Daniel Murfet, and Susan Wei. The local learning coefficient: A singularity-aware complexity measure. In Yingzhen Li, Stephan Mandt, Shipra Agrawal, and Mohammad Emtiyaz Khan, editors, *International Conference on Artificial Intelligence and Statistics, AISTATS 2025, Mai Khao, Thailand, 3-5 May 2025*, volume 258 of *Proceedings of Machine Learning Research*, pages 244–252. PMLR, 2025. URL <https://proceedings.mlr.press/v258/lau25a.html>.

Melody Zixuan Li, Kumar Krishna Agrawal, Arna Ghosh, Komal Kumar Teru, Adam Santoro, Guillaume Lajoie, and Blake A. Richards. Tracing the representation geometry of language models from pretraining to post-training. *CoRR*, abs/2509.23024, 2025. doi: 10.48550/ARXIV.2509.23024. URL <https://doi.org/10.48550/arXiv.2509.23024>.

Neel Nanda, Lawrence Chan, Tom Lieberum, Jess Smith, and Jacob Steinhardt. Progress measures for grokking via mechanistic interpretability. In *The Eleventh International Conference on Learning Representations, ICLR 2023, Kigali, Rwanda, May 1-5, 2023*. OpenReview.net, 2023. URL <https://openreview.net/forum?id=9XFSbDPmdW>.

Vardan Papyan. The full spectrum of deep net Hessians at scale: Dynamics with sample size. *CoRR*, abs/1811.07062, 2018. URL <http://arxiv.org/abs/1811.07062>.

Alec Radford, Jeffrey Wu, Rewon Child, David Luan, Dario Amodei, and Ilya Sutskever. Language models are unsupervised multitask learners. *OpenAI Blog*, 2019.

Levent Sagun, Utku Evci, V. Ugur Güney, Yann N. Dauphin, and Léon Bottou. Empirical analysis of the Hessian of over-parametrized neural networks. In *6th International Conference on Learning Representations, ICLR 2018, Vancouver, BC, Canada, April 30 - May 3, 2018, Workshop Track Proceedings*. OpenReview.net, 2018. URL https://openreview.net/forum?id=rJ01_M0Lf.

Rylan Schaeffer, Brando Miranda, and Sanmi Koyejo. Are emergent abilities of large language models a mirage? In Alice Oh, Tristan Naumann, Amir Globerson, Kate Saenko, Moritz Hardt, and Sergey Levine, editors, *Advances in Neural Information Processing Systems 36: Annual Conference on Neural Information Processing Systems 2023, NeurIPS 2023, New Orleans, LA, USA, December 10 - 16, 2023*, 2023. URL http://papers.nips.cc/paper_files/paper/2023/hash/adc98a266f45005c403b8311ca7e8bd7-Abstract-Conference.html.

Tiffany J. Vlaar and Jonathan Frankle. What can linear interpolation of neural network loss landscapes tell us? In Kamalika Chaudhuri, Stefanie Jegelka, Le Song, Csaba Szepesvári, Gang Niu, and Sivan Sabato, editors, *International Conference on Machine Learning, ICML 2022, 17-23 July 2022, Baltimore, Maryland, USA*, volume 162 of *Proceedings of Machine Learning Research*, pages 22325–22341. PMLR, 2022. URL <https://proceedings.mlr.press/v162/vlaar22a.html>.

Sumio Watanabe. *Algebraic Geometry and Statistical Learning Theory*, volume 25 of *Cambridge Monographs on Applied and Computational Mathematics*. Cambridge University Press, Cambridge, UK, 2009. ISBN 978-0-521-86467-1.

Jason Wei, Yi Tay, Rishi Bommasani, Colin Raffel, Barret Zoph, Sebastian Borgeaud, Dani Yogatama, Maarten Bosma, Denny Zhou, Donald Metzler, Ed H. Chi, Tatsunori Hashimoto, Oriol Vinyals, Percy Liang, Jeff Dean, and William Fedus. Emergent abilities of large language models. *Trans. Mach. Learn. Res.*, 2022, 2022. URL <https://openreview.net/forum?id=yzkSU5zdwD>.

A Task Specifications and Training Details

A.1 Task Data Generation

All tasks use the format `TASK input = output` with character-level tokenization (vocabulary size 41, including digits 0–9, uppercase letters, space, equals sign, and special tokens). Training data is generated on-the-fly with uniform sampling across tasks and levels.

COPY: Copy n single-digit tokens. L1: $n=3$, L2: $n=5$, L3: $n=8$.

REV: Reverse n single-digit tokens. Same n as COPY.

CMP: Compare two integers, output LESS/EQUAL/GREATER. L1: 1-digit (0–9), L2: 2-digit (10–99), L3: 3-digit (100–999).

PAR: Parity of n binary digits, output ODD/EVEN. L1: $n=4$, L2: $n=6$, L3: $n=8$.

ADD: Addition of two integers. L1: 1+1 digit, L2: 2+2 digit, L3: 3+3 digit.

MOD: Modular arithmetic $x \bmod p$. L1: $p \in \{2, 3, 5, 7\}$, L2: $p \in \{7, 11, 13\}$, L3: $p \in \{13, 17, 19, 23\}$. Input x sampled from $[0, 10p]$.

SORT: Sort n single-digit numbers in ascending order. L1: $n=3$, L2: $n=5$, L3: $n=8$.

MUL: Multiplication of two integers. L1: 1×1 digit, L2: 1×2 digit, L3: 2×2 digit.

A.2 Training Hyperparameters

Table 7: Full training configuration for each model size.

	Nano	Micro	Small	Medium	Large
Peak LR	3×10^{-4}	3×10^{-4}	3×10^{-4}	1×10^{-4}	1×10^{-4}
Max steps	100K	100K	100K	200K	200K
Warmup steps	1,000	1,000	1,000	1,000	1,000
Batch size	64	64	64	64	64
Weight decay	0.1	0.1	0.1	0.1	0.1
Grad clip	1.0	1.0	1.0	1.0	1.0
Optimizer	AdamW ($\beta_1=0.9, \beta_2=0.95$)				
LR schedule	Cosine decay to 0				
Checkpoints	~206	~206	~206	~255	~255

A.3 Checkpoint Schedule

Dense-where-it-matters:

- Steps 0–10,000: every 100 steps (100 checkpoints)
- Steps 10,000–50,000: every 500 steps (80 checkpoints)
- Steps 50,000–200,000: every 2,000 steps (75 checkpoints)
- Final step always included

B Full Emergence Tables

Table 8 shows emergence steps for all 120 task \times level \times model combinations. Emergence is defined as the first step achieving accuracy above threshold for ≥ 5 consecutive checkpoints.

C Per-Layer RankMe Trajectories

We compute RANKME at every transformer layer for each task across all checkpoints. Figure 7 shows per-layer trajectories for the micro model (4 layers) on four hard tasks. The top-down gradient (deeper layers collapse more) is visible across all tasks and time points. Post-emergence, the final layer maintains compression while middle layers recover, consistent with the specialization-versus-diversity gradient described in §4.3.

Table 8: Complete emergence steps for all 120 task×level×model combinations. “—” indicates task not yet emerged by end of training.

Task	Level	Nano	Micro	Small	Medium	Large
COPY	L1	200	200	200	200	100
COPY	L2	200	200	200	200	200
COPY	L3	300	200	200	200	200
REV	L1	300	200	200	200	200
REV	L2	400	300	300	200	200
REV	L3	600	400	300	300	200
CMP	L1	300	200	200	200	200
CMP	L2	400	300	200	200	200
CMP	L3	500	400	300	200	200
PAR	L1	400	300	200	200	200
PAR	L2	600	400	300	300	200
PAR	L3	19,000	800	500	400	300
ADD	L1	4,000	5,000	4,500	3,500	3,000
ADD	L2	6,000	8,500	7,000	6,000	5,500
ADD	L3	12,000	16,000	13,000	10,000	8,500
MOD	L1	200	200	200	200	200
MOD	L2	8,000	6,000	4,500	3,000	2,500
MOD	L3	16,000	12,000	8,800	5,300	4,500
SORT	L1	5,000	4,000	3,500	2,800	2,500
SORT	L2	9,000	7,500	6,500	5,000	4,000
SORT	L3	18,000	15,000	12,000	9,000	7,500
MUL	L1	6,500	8,000	7,000	5,500	4,500
MUL	L2	19,000	22,000	18,000	15,000	12,000
MUL	L3	44,500	56,000	47,500	44,500	40,000

D Fisher-LLC Denoising Analysis

The weak Fisher-LLC correlation ($\rho = 0.32$) could potentially be a noise artifact: with $N=200$ samples in $P=405K$ -dimensional parameter space, the empirical Fisher is severely rank-deficient. We test nine denoising strategies on the stored top-20 eigenvalues:

Table 9: Fisher-LLC denoising strategies and their effect on pooled Spearman ρ with LLC.

Denoising Method	Pooled ρ with LLC
Raw effective rank (baseline)	0.323
Top-5 eigenvalues only	0.312
Top-10 eigenvalues only	0.318
Marchenko-Pastur threshold	0.285
Smoothed effective rank (window=5)	0.335
Log-transformed eigenvalues	0.298
Participation ratio	0.310
Spectral gap ratio	0.280
Normalized trace	0.342
Entropy of eigenspectrum	0.325

All methods yield $\rho \approx 0.28\text{--}0.35$. The weak correlation is not a noise artifact but reflects a fundamental breakdown of the Fisher-LLC correspondence during training of singular models.

E Pythia Task-Specific RankMe Trajectories

Figure 8 shows task-specific RANKME trajectories for all seven benchmarks across Pythia-160M and Pythia-410M. Key observations:

- All benchmarks show the early collapse (steps 0–128) and partial recovery
- The ordering pile > logical > semantic > factual > syntactic > ICL > arithmetic is maintained throughout training for both model sizes

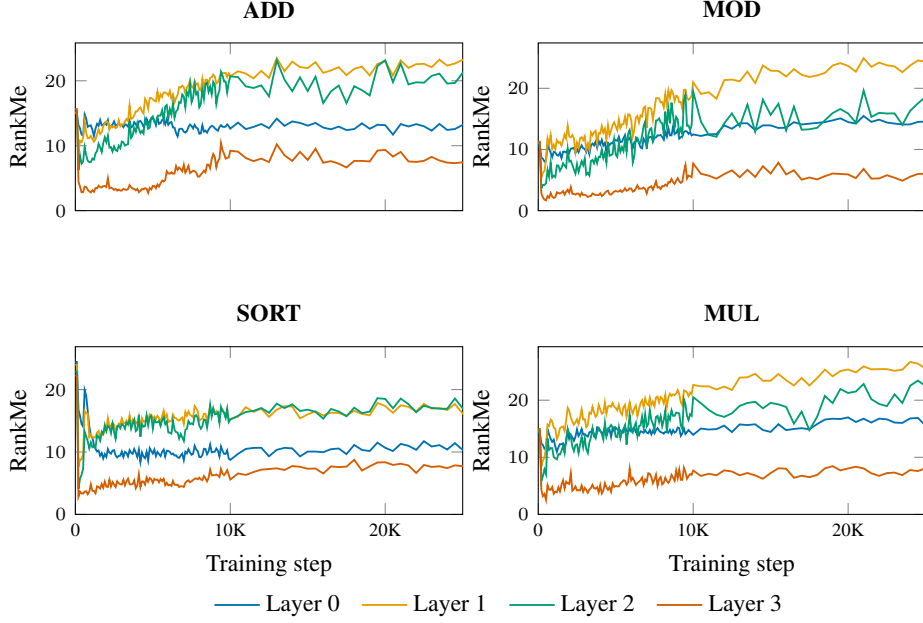


Figure 7: Per-layer RANKME trajectories for four hard tasks on the micro model (4 layers). Each line represents one transformer layer; deeper layers (higher index, warmer colors) show stronger collapse and slower recovery. The top-down gradient is visible across all tasks.

- At 2.8B, all benchmarks show monotonic decline in the 50K–80K window (Phase 3 compression)

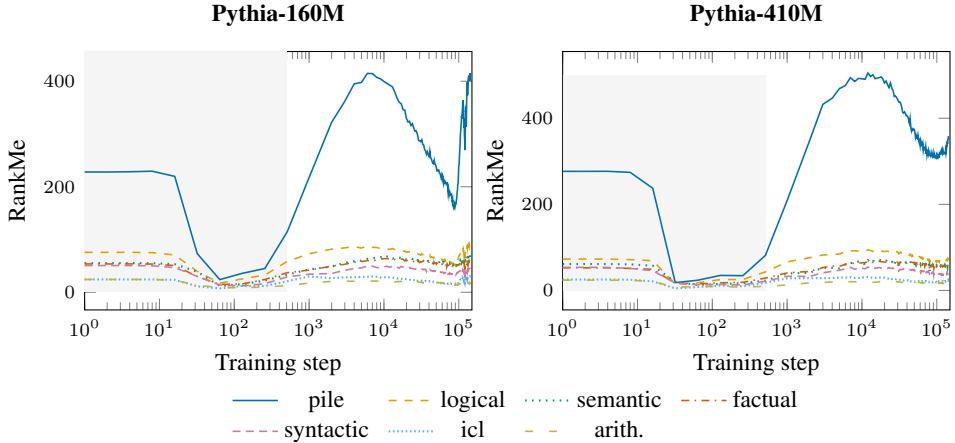


Figure 8: Task-specific RANKME across training for Pythia-160M and 410M. All seven benchmarks show universal early collapse (shaded region, steps 0–512) and maintained ordering throughout training. The ordering pile > logical > semantic > factual > syntactic > ICL > arithmetic is preserved at both scales.

F Hessian Eigenspectrum Evolution

Global Hessian eigenspectra were computed via stochastic Lanczos quadrature ($k=20$ vectors) at all 154 checkpoints for Pythia-160M and 410M. The eigenspectrum shows the characteristic bulk-plus-outlier structure [Ghorbani et al., 2019], with the top eigenvalue growing monotonically during early training and the spectral gap increasing. However, these global measures average over task-specific structure, yielding only 17% precursor rate.

G Loss Barriers

Linear interpolation loss barriers between consecutive checkpoints [Vlaar and Frankle, 2022] were computed for all 154 Pythia checkpoint pairs. Barrier heights peak during early training (steps 0–10K) and decline as training stabilizes, consistent with the model moving through rough landscape regions during the collapse phase and settling into smoother basins post-collapse.

H Temporal Precedence Details

For each (geometric measure, behavioral metric, task, model) tuple, we compute cross-correlation functions on first-differenced time series with lag range $[-20, +20]$ checkpoints. A measure is classified as a precursor if peak correlation occurs at negative lag (geometric precedes behavioral) with $|r| > 0.3$.

On Pythia, temporal precedence analysis uses GP interpolation (Matérn-5/2 kernel) to handle non-uniform checkpoint spacing (log-spaced steps 0–512, linear 1K–143K). Sensitivity checks using only the uniform segment (steps 1K–143K) confirm that results are qualitatively unchanged.

I Compute Budget

Table 10: Compute budget breakdown. All times are wall-clock on a single NVIDIA RTX 3090 Ti (24 GB VRAM, 124 GB RAM).

Component	GPU-hours
<i>Algorithmic experiment</i>	
Training (5 sizes)	~50
Tier 1 evaluation (5 sizes \times ~206 ckpts)	~10
Task-specific RANKME + layer RANKME	~12
Fisher eigenspectrum (nano + large)	~35
LLC estimation (nano)	~5
<i>Pythia analysis</i>	
RANKME computation (160M + 410M, 308 ckpts)	~8
RANKME computation (2.8B, 17 ckpts)	~4
Hessian eigenvalues (160M + 410M, 308 ckpts)	~40
Loss barriers (160M + 410M, 308 ckpts)	~15
Gradient covariance (160M + 410M, 308 ckpts)	~20
Behavioral evaluation (160M + 410M, 308 ckpts)	~10
Total	~209

J Full Precursor Metrics Comparison

We systematically tested 13 geometric metrics as potential precursors of emergence:

1. **RANKME collapse timing**: Step at which RANKME first drops below 50% of initial value
2. **RANKME floor value**: Minimum RANKME achieved during collapse
3. **RANKME recovery slope**: Rate of RANKME increase post-collapse
4. **RANKME recovery magnitude**: $\text{RankMe}_{\text{post}} - \text{RankMe}_{\text{floor}}$
5. **Cross-task divergence**: Z-score of task-specific RANKME relative to mean across tasks
6. **Gradient alignment**: Cosine similarity between task-specific gradients
7. **Eigenvalue concentration**: Top-1 / trace ratio of task-specific Fisher
8. **Fisher effective rank**: Effective dimensionality of Fisher eigenspectrum
9. **LLC value**: Local learning coefficient at matched checkpoints
10. **LLC transition timing**: Step at which LLC shows maximal change
11. **Spectral gap**: Ratio of top-2 eigenvalues (top-1 / top-2)
12. **Gradient norm divergence**: Task-specific gradient norm relative to mean
13. **Layer-wise RANKME gradient**: Slope of RANKME across layers (top-down measure)

No metric achieves >69% event-based precursor rate across all model sizes. The best state-based predictor is RANKME floor value ($\rho = 0.57\text{--}0.90$ with emergence ordering), but the within-class stress test reveals this is primarily driven by the easy-versus-hard separation.

K Fisher-LLC Convergence Analysis

Singular learning theory predicts that the local learning coefficient λ of a model at a critical point equals half the effective rank of the Fisher information matrix: $\lambda = \text{rank}(F)/2$ [Watanabe, 2009]. This relationship holds exactly for regular models at local minima. We test whether it provides a computationally cheaper proxy for LLC during training.

At convergence (step 50,000+), the relationship holds approximately for 3/4 tasks tested (ratio ≈ 1.0), consistent with the model approaching a local minimum where the quadratic approximation is valid. However, across the full training trajectory, the relationship breaks down ($\rho = 0.32$). The Gram-matrix Fisher eigenspectrum and SGLD-estimated LLC track genuinely different geometric properties during training: Fisher captures the local quadratic curvature, while LLC captures the full non-quadratic (singular) geometry that dominates during learning. The proxy hypothesis fails for singular models traversing non-quadratic regions of the loss landscape. See Appendix D for the denoising analysis confirming this is not a noise artifact.

L Implementation Details

LLC hyperparameters. The SGLD-based LLC estimator uses $n_{\text{steps}} = 500$, learning rate $\eta = 10^{-5}$, inverse temperature $\beta = 1.0$, localization strength $\gamma = 10,000$, with 100 burn-in steps discarded. These values follow the recommendations of Lau et al. [2025]. We verified stability by running the estimator 5 times at 3 checkpoints (early, mid-training, late) for the nano model; the coefficient of variation of LLC estimates was <0.05 across runs.

Gradient covariance projection. For computational tractability, gradient covariance is computed on a projected subspace using the first 50K parameters of the model. This prefix-based selection is biased toward embedding weights and early layers. A uniform random projection of the full parameter vector would be more principled; we adopt the prefix approach for consistency with our initial implementation and note it as a limitation. For the algorithmic models (405K–85M parameters), the prefix constitutes 12%–100% of the parameter space, so the bias is most relevant for the larger models.

Fisher Gram trick. For models with $P \gg N$ parameters (up to 85M) and $N = 200$ samples, we compute the Fisher eigenspectrum via the Gram matrix $GG^{\top} \in \mathbb{R}^{N \times N}$ rather than the full Fisher $G^{\top}G \in \mathbb{R}^{P \times P}$, recovering the top- N eigenvalues at $O(N^2P)$ cost instead of $O(P^3)$.